Registry No. NaCl, 7647-14-5; Separan AP273, 37224-28-5; Polyox WSR, 25322-68-3.

References and Notes

(1) Ogston, A. G.; Woods, E. F. *Trans. Faraday Soc.* **1954**, *50*, 635.
(2) Mijnlieff, P. F., Jaspers, W. J. M. *Trans. Faraday Soc.* **1971**, *67*, 1837.
(3) Brochard, F.; de Gennes, P.-G. *Macromolecules* **1977**, *10*, 1157.
(4) Roots, J.; Nystrom, B. *Polymer* **1979**, *20*, 148.
(5) Roots, J.; Nystrom, B. *Chem. Scr.* **1980**, *15*, 165.
(6) Nystrom, B.; Boileau, S.; Hemery, P.; Roots, J. *Eur. Polym. J.* **1981**, *17*, 249.
(7) Ethier, C. R. *Biorheology* **1986**, *23*, 99.
(8) Pouyet, G.; Francois, J.; Dayantis, J.; Weill, G. *Macromolecules* **1980**, *13*, 176.
(9) Roots, J.; Nystrom, B. *Polymer* **1981**, *22*, 573.
(10) Jackson, G. W.; James, D. F. *Biorheology* **1982**, *19*, 317.
(11) Spielman, L.; Goren, S. L. *Environ. Sci. Technol.* **1963**, *2*, 279.
(12) Chesneau, C. P. M.A.Sc. Thesis, University of Toronto, 1985.
(13) Kulicke, W.-M.; Kniewske, R.; Klein, J. *Prog. Polym. Sci.* **1982**, *8*, 373.
(14) Kimbell, D. G. M.A.Sc. Thesis, University of Toronto, 1987.
(15) Brandrup, J.; Immergut, E. H. *Polymer Handbook*, 2nd ed.; Wiley: New York, 1975.

Morphology of Segmented Polybutadiene–Polyurethane Elastomers

Chi Li,† Steven L. Goodman,‡ Ralph M. Albrecht,‡ and Stuart L. Cooper*,†

Department of Chemical Engineering and Department of Veterinary Science, University of Wisconsin, Madison, Wisconsin 53706.

Received October 20, 1987

ABSTRACT: The morphology of segmented polybutadiene–polyurethanes containing a wide range of hard-segment content was studied with high-voltage electron microscopy (HVEM), high resolution scanning electron microscopy (SEM), and small-angle X-ray scattering. Specimens were prepared by thin film casting from solutions and by ultramicrotomy of bulk materials. Segmented polyurethanes with low hard-segment content have a morphology of dispersed, short, hard-segment cylinders embedded in a matrix of polybutadiene soft segments. An alternating hard- and soft-segment rodlike or lamellar microdomain structure was characteristic of materials with higher hard-segment contents. The length of lamellae or rods increased with increasing hard-segment content while the width of the lamellar or rodlike microdomains remained constant. At very high hard-segment contents, a morphology having a dispersed soft-segment phase was observable. It was also found that the shape of the dispersed soft-segment microdomains in the high hard-segment content samples was related to the details of sample preparation. The spacing between the hard- and soft-segment microdomains measured from micrographs was found to correlate well with the long spacing calculated from SAXS curves. In some cases the same sample was viewed by using HVEM and both secondary and backscattering electron imaging in the high-resolution SEM. The observation of similar morphologies with techniques based on such different imaging physics supports the contention that the structures are real and not a result of instrumental artifacts.

Introduction

The micromorphology of phase-separated polyurethane block copolymers and its influence on physical properties has been a focal point of much structure-property research.[1-7] Considerable attention has been devoted to characterization of the microdomains of the soft- and hard-segment phases since Cooper and Tobolsky postulated a phase-separated structure for segmented polyurethanes.[1] The first direct evidence for the formation of a two-phase structure was from the small-angle X-ray scattering (SAXS) studies by Bonart[8] and Clough et al.[9] SAXS profiles of polyether- and polyester-based polyurethanes show a prominent scattering peak at low angle, corresponding to a long spacing of about 10–25 nm.[10-13] This spacing was interpreted as being related to the interlamellar distance between microdomains.[11-13] On the basis of these observations, several models which describe the two-phase morphology have been proposed.[3,7,14,15] Since segmented polyurethanes possess a disordered two-phase morphology, detailed structural information on polyurethane morphology, however, cannot be derived from their single-peak X-ray scattering profiles without ambiguity.

Transmission electron microscopy (TEM) has been carried out on many polyurethane material systems. Both solvent casting and ultramicrotomy techniques have been employed to prepare thin films for TEM observation.[14,16-19] Ultramicrotomy can provide representative thin sections of the bulk morphology of the elastomer, but the low soft-segment glass transition temperature (T_g) requires cutting to be carried out with difficulty at very low temperatures. Thin films prepared by solvent casting techniques, on the other hand, may not represent the bulk morphology of the block copolymer since the process of phase separation depends upon the casting solvent and other conditions.[20] Lack of mass-thickness (atomic density) contrast between the hard- and soft-segment phases can cause imaging artifacts in the electron microscope as a result of poor focusing.[21,22] Osmium tetroxide has been used to selectively stain chemically unsaturated moieties in order to provide contrast between the hard- and soft-segment phases.[23] Recently, phosphotungstic acid (PTA) has been successfully applied to stain the amorphous region of polyamide materials.[24] An additional difficulty with electron microscopy of polyurethanes is that radiation damage and heating can cause the material to degrade. High-voltage electron microscopy (HVEM, a TEM at 1.0-MeV accelerating potential as compared to 100 keV in conventional TEM) reduces radiation damage to the polymer specimen due to decreased electron absorption.[25] This provides the opportunity for high-resolution electron microscopy. Additionally the ability to view selected areas of the sample at several angles of specimen tilt in the HVEM allows investigation of the sample's three-dimensional structure.[25]

Scanning electron microscopy (SEM) has been primarily used to investigate the surface topography of polymeric materials.[26] The bulk morphology of polymers can also

* Author to whom correspondence should be addressed.
† Department of Chemical Engineering.
‡ Department of Veterinary Science.

0024-9297/88/2221-2367$01.50/0

be studied with SEM by viewing fracture surfaces, although interpretation of the SEM image of such a surface can be very difficult. Conventional SEM cannot provide sufficient resolution for the characterization of polyurethane microphase structure, although Foks and Michler, using SEM and TEM, described inhomogeneities as large as several microns and a spherulitic superstructure in a series of polyester–polyurethanes.[27] A newly designed low-voltage SEM equipped with both secondary electron and backscattered electron (BSE) detectors can provide adequate resolution for block copolymer morphology characterization. BSE imaging detects the signal of incident electrons that are scattered backward by the sample. The intensity of backscattering is a strong function of the sample's atomic density under the incident scanning electrons. Thus, OsO_4-stained polybutadiene soft-segment microdomains in a polyurethane block copolymer can be readily viewed by a high-resolution BSE imaging SEM. To the best of our knowledge, BSE imaging SEM has not been previously applied to investigate the morphology of segmented polyurethane elastomers.

Highly phase-separated polyurethanes based on polybutadiene soft segments provide good model materials for studying the morphology and structure-property relationship of multiblock copolymers.[13,29-31] Chen-Tsai et al. and Serrano et al. have investigated the morphology of polybutadiene–polyurethanes containing amorphous hard segments (based on toluene diisocyanate and butanediol).[30,31] Their results indicated that a lamellar morphology exists when the hard-segment weight fraction in the block copolymer is about 0.5.[30,31] They observed that the morphology changed to dispersed cylinders of polybutadiene soft segments embedded in a hard-segment matrix when the hard-segment content reached 0.7. At hard-segment weight fractions below 0.5, they reported that no reliable information about the structure of the block copolymer could be derived from their phase contrast imaging micrographs.[30,31] Due to the nature of the phase contrast imaging, Serrano et al. could not determine the morphology in three dimensions.[31] Also a recent study of polybutadiene–polyamide multiblock copolymer structure reported a disordered lamellar morphology.[32] Recently, high-voltage electron microscopy and high-resolution scanning electron microscopy have been used to investigate the surface and bulk microphase separation of segmented polyurethanes for biomedical applications.[33,43]

In this study, several direct and indirect techniques were used to study the morphology of polybutadiene–polyurethane block copolymers. Ultramicrotomed thin sections as well as thin film samples cast from solvent were viewed by using a high-voltage transmission electron microscope operated at 1 MeV to reduce electron radiation damage. Multiple-tilt images were recorded to derive the shape of the microdomains in three dimensions. Digital image processing and analysis was performed to quantify the dimensions of the microdomains. A high-resolution field emission scanning electron microscope equipped with both secondary and backscattered electron detectors provided additional detail on the phase-separated micromorphology of the polybutadiene–polyurethanes. Small-angle X-ray scattering (SAXS) experiments were also performed on bulk polymer samples. For further correlation of the microdomain dimensions derived from electron microscopy with results obtained by SAXS, optical diffraction experiments were carried out on selected HVEM micrographs.

Experimental Section

Polybutadiene–Polyurethane Synthesis. Segmented polybutadiene–polyurethane block copolymers were synthesized by using standard urethane chemistry in a solvent mixture of tetrahydrofuran (THF) and dimethylacetamide (DMAc).[35] The synthesis procedure has been fully documented.[36,37] Hydroxyl-terminated polybutadiene oligomers (HTPBD) of molecular weights 2000 and 3000 as well as their molecular characterization data were kindly provided by Dr. Suichi Matsumoto of Japan Synthetic Rubber Co. Ltd. The functionality of the oligomers was approximately 1.98 while the ratio of 1,2- to 1,4-butadiene repeating units was 43:57. Diphenylmethane diisocyanate (MDI) was purchased from Polysciences Inc. and was purified by recrystallization. 1,4-Butanediol (BD), THF, and DMAc were acquired from Aldrich Chemical Co. and dehydrated by distillation or by using molecular sieves (Fisher Scientific, type 4A). The hard-segment weight fraction and the polystyrene equivalent number-average molecular weight (measured by GPC) of each of the polymer samples synthesized are shown in Table I. The sample code describes the soft-segment molecular weight and weight percentage of hard segment in each material. For example, PBD-3-62 indicates that the soft segment in the sample is HTPBD 3000 and the hard-segment content in the sample is 62% by weight. The hard-segment phase volume fraction of each material was estimated by assuming complete phase separation with 0.98 g cm^{-3} soft-segment-phase mass density and 1.30 g cm^{-3} hard-segment-phase mass density.[12,13]

Table I
Sample Specification

sample	W_h, %	EM sample preparation	$10^{-4}M_n$
PBD-3-31	31.3	solvent cast	5.1
PBD-3-42	42.0	solvent cast	6.2
PBD-3-49	48.5	solvent cast	3.7
PBD-3-58	57.8	solvent cast/ultramicrotomed	4.5
PBD-3-62	61.9	solvent cast/ultramicrotomed	3.2
PBD-3-67	67.2	solvent cast/ultramicrotomed	4.0
PBD-2-75	74.7	solvent cast/ultramicrotomed	2.9
PBD-3-75	75.3	solvent cast/ultramicrotomed	2.7

Sample Preparation. Polybutadiene–polyurethane films of 0.5–1.0 mm thickness were cast from DMAc solutions and vacuum dried at room temperature for 1 week. These thick films were used for the SAXS experiments and also served as bulk samples for ultramicrotomy. Thin films for HVEM were prepared by spin casting 0.2% PBD–polyurethane in DMAc solution onto a NaCl single-crystal plate using a technique developed by Goodman and Albrecht.[38] The NaCl substrate was removed by dissolving it in distilled water, such that a thin polymer film remained on the water surface. Profilometry measurements indicated that the thin films varied from 20 to 80 nm thick. The thin films were transferred onto 500- or 1000-mesh copper TEM grids and vapor stained with OsO_4 (from a 4% solution) for 4 h. Colloidal gold particles (5-nm) were then deposited on the thin films to assist focusing and to provide a size standard.[38] All EM samples were stored under vacuum to minimize contamination.

Thin sections of polybutadiene–polyurethanes were obtained by ultramicrotomy. Bulk polymer samples were cut into 0.5 × 0.5 × 5.0 mm strips and embedded in a room-temperature curing epoxy resin (Emary Co.). The samples were sectioned by using a Sorvall Microtome MT2B device equipped with a diamond knife and a cryo kit. Cutting of the high hard-segment content materials (PBD-3-75, PBD-2-75, PBD-3-67) was carried out at room temperature with a wet knife while the other materials were microtomed at −60 °C with a dry knife. Optical reflection indicated that these sections were about 40 nm thick. Thin sections of each sample were then transferred onto 500-mesh Cu TEM grids and vapor stained with OsO_4 from a 4% solution for 4 h. The thin sections were then rinsed, dried, and stored under vacuum prior to electron microscopy observation.

Electron Microscope Facility. Thin films, and sections of polybutadiene–polyurethanes, were viewed in the University of Wisconsin—Madison, NIH Bioresource's AEI EM7 MkII high-voltage electron microscope.[25] All observations were at 1.0-MeV accelerating potential. The HVEM bright field images were recorded on to Kodak 4199 or SO-163 photographic films through either a 30 μm or a 10 μm objective aperture with magnifications ranging from 30 000 to 316 000. To minimize the electron dose in the HVEM, a low light level (SIT) video camera with a digital

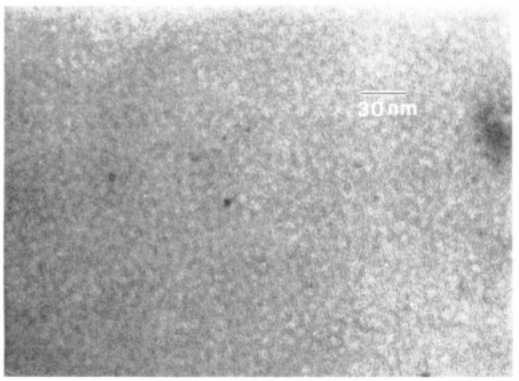

Figure 1. HVEM micrograph of an OsO_4-stained PBD-3-31 film cast from solution.

image enhancement/memory system was used for all sample viewing except photographic exposure.[25] The range of electron dosage was from 1800 to 45 000 electrons nm^{-2}.[25] No visible alterations in polymer structure were observed during the HVEM focusing and viewing process. Most micrographs were recorded at critical focus or very slight under focus (<5 nm). The memory and differential function of the digital image processor made possible almost perfect image alignment of the same area viewed at different tilt angles.[25]

A Hitachi S-900 high-resolution scanning electron microscope with secondary and backscattered electron detectors was also used for viewing the morphology of the segmented polybutadiene polyurethanes. The instrument was designed for exceptionally high resolution (better than 0.8 nm at 30 kV) and has been modified for enhanced low-voltage performance (3–5 nm at 1.0 keV).[39] OsO_4-stained thin films and sections on TEM grids were viewed without conductive metal coating. SEM micrographs were recorded at 1.0–20 keV accelerating potentials and 30 000 to 100 000 magnifications.

Small-Angle X-ray Scattering. Small-angle X-ray scattering was performed by using X-rays produced by a rotating anode generator operating at 35-kV potential and 10-mA emission current. X-ray wavelength was predominately 0.1542 nm (Cu Kα). A modified compact Kratky SAXS camera was used to collimate the X-ray into a beam which was 1.0 cm by 100 μm at the sample. Suitable corrections for detector sensitivity, detector dark current, parasitic scattering, slit length smearing, and sample absorption were made. Relative intensity data were converted to absolute intensity by using a Lupolen (polyethylene) standard. The range of linear attenuation coefficients was about 0.4–0.6 mm^{-1}. Detailed descriptions of the SAXS facility and data processing procedure can be found elsewhere.[12,13]

Optical Diffractometry. An optical diffractometer equipped with a He–Ne laser (632.8-nm wavelength) was used to obtain the optical diffraction patterns from HVEM micrographs. The contrast of the micrographs was enhanced, and the size of the recorded microdomains was reduced by using photographic means in accordance with the geometry of the light scattering apparatus. The profile of relative scattering intensity $I(q)$ versus the scattering vector q was derived from the optical diffractograms by using a digital image analyzer with software for radial averaging. The scattering vector $q = (4\pi \sin \theta)/\lambda$ where θ is the scattering half angle and λ is the wavelength of the scattering radiation.

Digital Image Analysis. In addition to the digital image processor connected to the HVEM, a separate image analyzer was used to digitize the HVEM and SEM micrographs for subsequent quantification of microdomain spacings and morphology. This unit was also used to quantify the scattering intensity as a function of the scattering vector. The hardware of the image analysis system consisted of a video camera (NewVicon, Dage-MTI Inc.), a 512 × 512 pixel image digitizer/processor (PC Vision Plus, Imaging Technology Inc.), and an IBM-PC/AT compatible microcomputer based on an Intel 80386 processor. In-house developed software was used for image analysis.

Results and Discussion

Figures 1 and 2 show a series of HVEM micrographs of OsO_4-stained PBD-3-31 thin films cast from a 0.2% DMA solution. Considering the low volume fraction of hard segments (minority phase, volume fraction = 0.27), one would expect to observe a morphology of dispersed hard-segment spheres in this sample. The dispersed sphere morphology has been observed in many diblock and triblock copolymer systems at low volume fractions of one of the phases.[20] The observed morphology of PBD-3-31, however, can better be described as dispersed, disordered nonspherical hard-segment domains embedded in a soft-segment matrix. In some regions, very short, alternating dark and bright short stripes are observable. These short stripes can be the projection image of alternating hard- and soft-segment lamellae or short cylinders. The spacing of the phase-separated structure, measured as the sum of the widths of the dark and the bright stripes, is about 10 nm. The size distribution of the microdomain spacings seems to be narrow. This suggests that the morphology in this sample may represent the onset of a bicontinuous network structure. The bicontinuous morphology is defined here as a structure consisting of two separated but individually interconnected phases in three dimensions.[42] Gas diffusion measurements presented previously showed a threshold at about 0.35 hard-segment weight fraction where the effective gas diffusivity started to decrease significantly.[35] That observation suggests the formation of a continuous hard-segment microdomain structure which would increase the tortuosity of gas diffusion pathways through the more permeable soft-segment phase.[35] Although the MDI-BD hard-segment phase is semicrystalline, no spherulitic su-

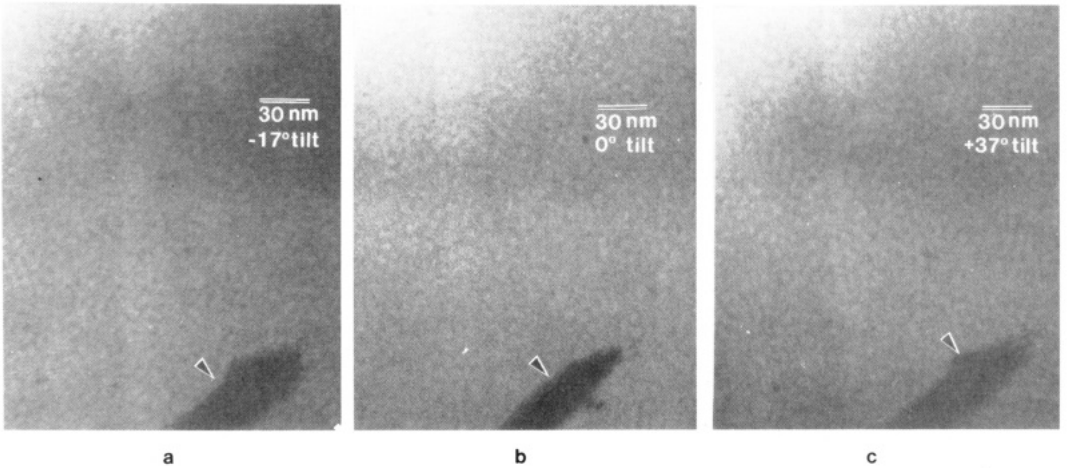

Figure 2. HVEM micrographs of an OsO_4-stained PBD-3-31 thin film at different specimen tilt angles; the dark spot on the bottom was used for image alignment: (a) −17° tilt, (b) 0° tilt, (c) +37° tilt.

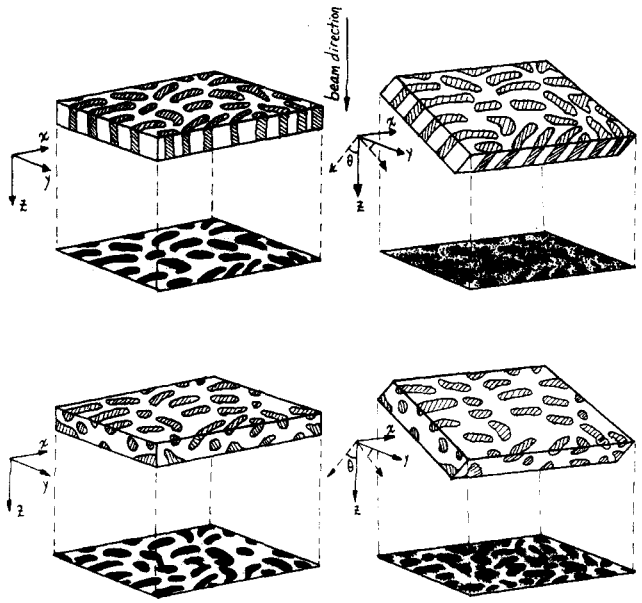

Figure 3. Illustration of the projection of morphology when HVEM specimens are tilted at different viewing angles: (a) dispersed microdomains are relatively insensitive to tilting; (b) lamellar microdomains become smeared by tilting.

perstructure was observed in any of the samples examined in this study.

The absence of an isolated spherical hard-segment microdomain morphology in PBD-3-31 may be attributed to the multiblock structure of segmented polyurethanes as well as their segmental ordering and hydrogen-bonding capability. Hydrogen bonding and crystallization of the MDI-BD hard segments tend to form platelike or cylindrical structures during the phase separation process.[3,4] Since PBD-3-31 exhibits hard-segment crystallinity as measured by DSC and a high degree of interurethane hydrogen bonding as determined by infrared spectroscopy,[35] platelike or cylindrical hard-segment microdomains are more likely to be present.

The HVEM bright field images are two-dimensional projections of a three-dimensional structure. Thus, Figure 1 alone is insufficient to determine whether the morphology of PBD-3-31 consists of small plates or short cylinders of hard segments. However, projections of the sample morphology at different tilt angles (−17°, 0°, and +37°) help to resolve this question (Figure 2a–c). An effort was also made to study the morphology in three dimensions by stereoimaging. However, when the micrographs were viewed as stereopairs, stereoimaging did not provide conclusive information due to insufficient contrast for reliable stereoviewing. The large tilt-angle micrographs do reveal that the projected image of the morphology does not change with sample tilting, as shown in Figure 2a,c. This leads to the conclusion that the structure can be best described as a set of macroscopically disordered short hard-segment cylinders. A model incorporating these features is shown in Figure 3. A set of alternating hard- and soft-segment plates or dispersed hard-segment cylinders embedded in a soft-segment matrix would project similar HVEM images. However, their orientations in three dimensions would be significantly different as they represent different morphologies. A tilted specimen possessing a lamellar morphology would produce an image containing an unrecognizable area in contrast to the alternating dark and bright stripes observed at zero tilt, while projection of a sample containing randomly oriented dispersed cylinders will remain relatively insensitive to sample tilt, producing similar images at different angles.

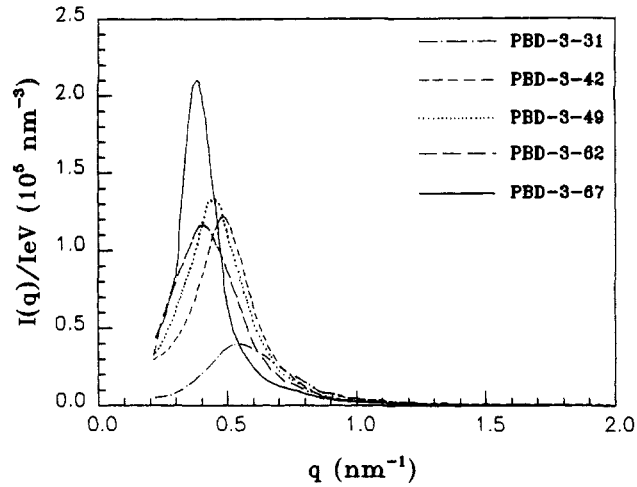

Figure 4. SAXS curves for PBD-3-31, PBD-3-42, PBD-3-49, PBD-3-62, and PBD-3-67. $I(q)/I\mathrm{eV}$ is the absolute scattering intensity, and q is the scattering vector.

However, it is also necessary to consider that sample thickness can play an important role in the projected image. Projections from thicker samples at high tilt angles tend to be more smeared because specimen tilting also increases the actual electron path length.

Small-angle X-ray scattering profiles of five of the materials examined are shown in Figure 4. Each scattering profile exhibits a single well-defined scattering peak characteristic of a periodic variation in electron density within the sample. The average of the repeat distance of the electron density variation can be estimated roughly from the position of the peak by using Bragg's law

$$\lambda = 2L \sin \theta \tag{1}$$

where L is known as the long spacing. In terms of the scattering vector q, this is equivalent to

$$L = 2\pi/q_{\mathrm{peak}} \tag{2}$$

where q_{peak} is determined from the maximum of the scattering profile or from the maximum of a plot of $q^2I(q)$ versus q in order to correct for the Lorentz factor.[34] In reality, the position of the peak position depends in a complex way on the arrangement as well as the structure of each scattering phase; the long spacing obtained from the application of Bragg's law is therefore not a well-defined physical dimension of the polymer structure, but it does indicate the scale of the electron density variation related to the microdomain spacing.[34]

The small-angle X-ray scattering profile of PBD-3-31 in Figure 4 shows a well-defined scattering peak at q = 0.590 nm^{-1}, which translates to a long spacing of 10.64 nm. The absence of multiple scattering peaks confirms the absence of a highly ordered structure (for example, monodisperse hard-segment spheres) in PBD-3-31. Since the HVEM micrographs indicate that the micromorphology of this material may not be described as lamellar, the long spacing should not be interpreted as the average separation distance of the microdomains. A polydisperse Percus-Yevick hard-sphere liquid model was used by Chen-Tsai et al. to fit their SAXS curves of a polybutadiene–polyurethane copolymer with similar hard-segment concentration.[30,40] It is not suitable, however, to apply the same model to fit our SAXS data since the HVEM micrographs show no evidence for a spherical hard-segment microstructure.

Alternating dark and bright stripes of OsO_4-stained PBD soft-segment and unstained urethane hard-segment microdomains, are clearly observed in many areas in the

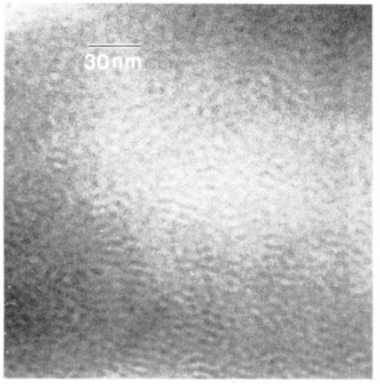

Figure 5. HVEM micrographs of an OsO_4-stained PBD-3-42 thin film cast from solution. A well-organized lamellar/rod-like morphology is observable.

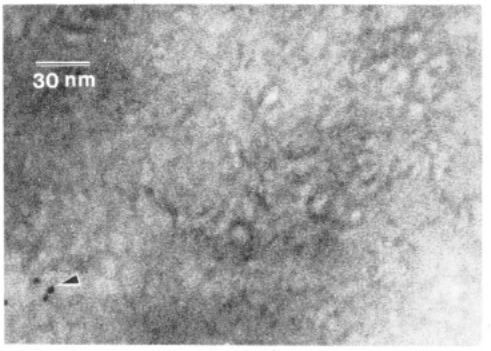

Figure 6. HVEM micrograph of an OsO_4-stained PBD-2-48 thin film cast from solution. A lamellar morphology is observable.

HVEM micrographs of PBD-3-42, PBD-3-49, PBD-3-62, and PBD-3-67 shown in Figures 5–8. (The observed morphology of PBD-3-58 is very similar to that of PBD-3-62 so the former is not shown.) Although the MDI-BD hard-segment phase is semicrystalline, no spherulitic superstructure was observed from any specimens in this series of samples. To illustrate the difference between the so called TEM "phase grain" artifacts and the polyurethane morphology, a HVEM micrograph of an unstained PBD-3-62 thin film recorded at a significantly underfocused condition is shown in Figure 7b. The "phase grain" image fails to provide any meaningful information about the polymer morphology. The alternating stripes are interpreted as characteristic of a lamellar or rodlike morphology in PBD-3-42, PBD-3-49, PBD-3-62, and PBD-3-67 prepared either by ultramicrotomy or by casting. Compared to the morphology in PBD-3-31, the lamellar or rod structure becomes well-defined in these samples since they have higher hard-segment volume fractions. In addition, the width of the alternating stripes does not vary significantly with hard-segment content. The average interlamellar spacing (measured as the sum of the widths of soft and hard segment microdomains) is 11 nm in PBD-3-42, 14 nm in PBD-3-62, and 14 nm in PBD-3-67, respectively (Table II). The interlamellar spacing in these segmented polybutadiene polyurethanes shows a strong dependence on soft-segment molecular weight with little dependence on the hard-segment content due to a high degree of phase separation. However, the lamellae or rod length increases significantly with increasing hard-segment content. Since the micrographs are two-dimensional projections of the morphology, it is difficult to calculate the exact length of the lamellae or long rods.

Interlamellar spacings of PBD-3-42, PBD-3-49, PBD-3-58, PBD-3-62, and PBD-3-67 can also be calculated from the SAXS data. In order to interpret the SAXS data of these materials correctly, the geometric symmetry of lamellar structure must be taken into account when calculating the long spacings.[30,34] The Lorentz factor corrected long spacings of PBD-3-42, PBD-3-49, PBD-3-58, PBD-3-62, and PBD-3-67, reported in Table II as an average interlamellar distance, agrees well with those measured from the electron micrographs.

Figure 8b is a high-resolution backscattered electron SEM micrograph of a thin, OsO_4-stained, PBD-3-67 film sample prepared by solvent casting. Similar to the HVEM

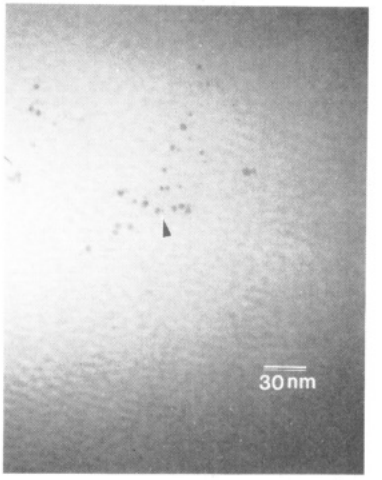

a

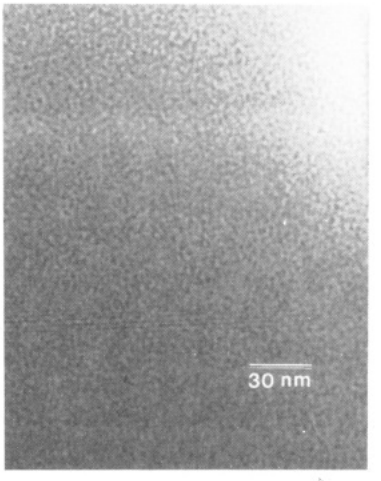

b

Figure 7. HVEM micrographs of PBD-3-62: (a) an OsO_4-stained cast film showing a lamellar/rod morphology (the very dark circles are projected images of the 5-nm gold particles); (b) an unstained thin film cast from solution at a significantly underfocused condition to produce so called "phase grain" imaging artifact.

Table II
Microdomain Spacings Measured from SAXS and HVEM[a]

sample	V_h	morphology	L, nm	d_i, nm	d_{is}, nm
PBD-31-31	0.27	short cylinders	10.6	9.5	
PBD-3-42	0.35	lamellar/rod-like	12.2*	11	
PBD-3-49	0.43	lamellar	12.9*	12	
PBD-3-58	0.51	lamellar/rod-like	12.7*	13	13
PBD-3-62	0.55	lamellar/rod-like	14.1*	14	14
PBD-3-67	0.61	lamellar/rod-like	16.8*	14	14
PBD-2-75	0.68	cylindrical/plate-like	22.3	27	21
PBD-3-75	0.68	cylindrical/plate-like	27.1	31	24

[a] V_h = hard segment phase volume fraction. L = long spacing from SAXS curve; the asterisk denotes Lorentz factor correction. d_i = microdomain spacing from HVEM micrograph of thin films. d_{is} = microdomain spacing from HVEM micrograph of thin sections.

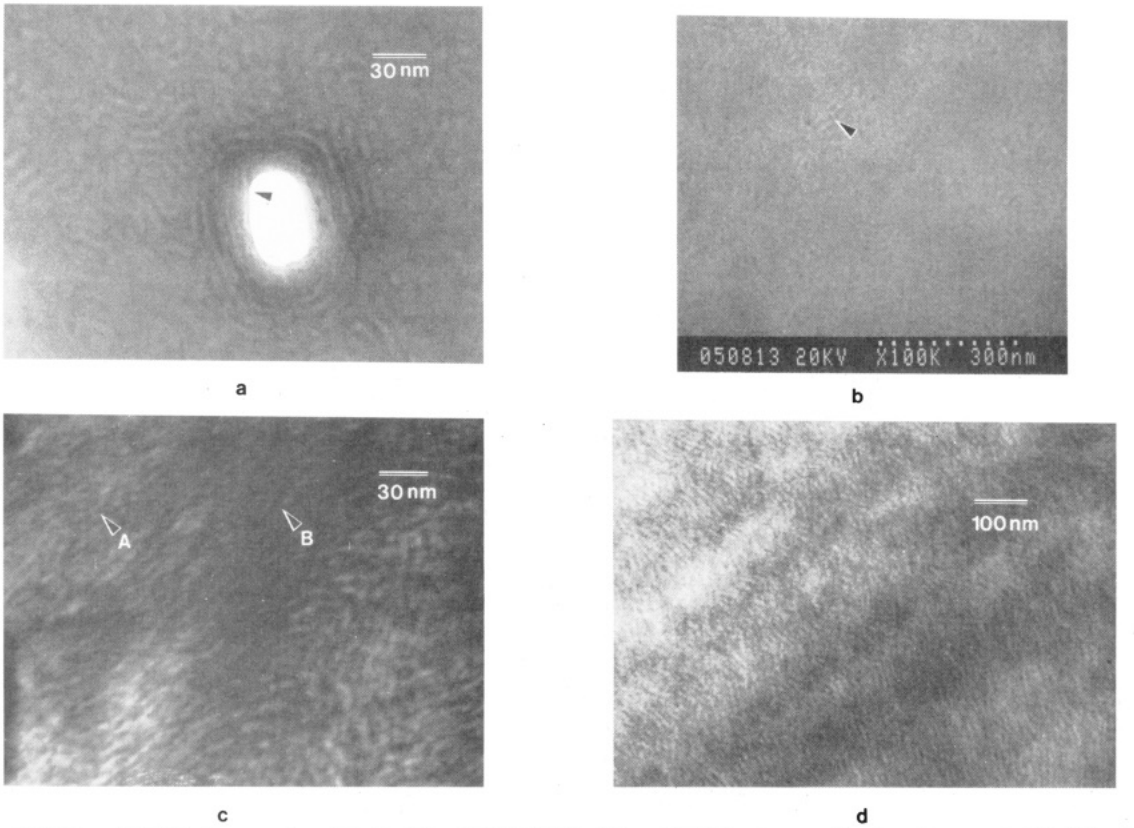

Figure 8. HVEM and SEM micrographs of OsO_4-stained PBD-3-67: (a) an HVEM micrograph of a solvent cast thin film (the bright circular area in the center is an image of a hole in the specimen; a lamellar structure is seen to develop around the hole), (b) an SEM BSE image recorded at 20-kV accelerating potential, (c) an HVEM micrograph of an ultramicrotomed thin section, (d) an HVEM bright field image of the same ultramicrotomed section observed at a low magnification.

micrograph shown in Figure 8a, alternating bright and dark stripes representing a lamellar or rodlike morphology are observable. The agreement between the morphology observed in PBD-3-67 using both SEM and HVEM is excellent. Since both the SEM and the HVEM reveal similar morphology in this material, imaging artifacts appear unlikely. Chen-Tsai et al. and Serrano et al. have successfully applied phase contrast imaging to view the morphology of unstained PBD–polyurethanes.[30,31] Their TEM images also revealed a similar lamellar structure present in a sample containing 52% hard segments.

While solvent cast thin films are useful in determining the general features of segmented polyurethane morphology, they cannot be used to investigate the fine structure of the bulk morphology in three dimensions. In addition, thin film casting may cause the microdomains to form specific orientations with respect to the film surface.[41] Thus, in order to check for some of these effects on sample morphology, ultramicrotomy was employed to produce thin sections for HVEM and SEM. Parts b and c of Figure 8 show HVEM micrographs of an OsO_4-stained thin section of PBD-3-67 prepared by ultramicrotomy. The comparison of HVEM images of both cast films and ultramicrotomed thin sections revealed no dramatic differences, although micrographs of ultramicrotomed thin sections of PBD-3-67 suggest that the microdomain structure of that material may be better described as long rods rather than lamellae. The small dark circles in some areas are suggested as revealing the rod cross section while the alternating dark and bright stripes show a view parallel to the rod's long dimension. Ultramicrotomed PBD-3-58 and PBD-3-62 thin sections possess a similar long rod morphology. A rodlike morphology has also been observed in several diblock and triblock copolymer systems.[20,42] An additional difference between the ultramicrotomed and thin cast samples was that the alternating stripes in the cast films appear to have a more uniform width and sharper edges suggesting a higher level of phase separation. This result is hardly surprising because of the lower viscosity during the initial stages of microphase separation allowing for more efficient development of the morphology (which may or may not be an equilibrium structure).

Figures 9 and 10a are HVEM micrographs of thin film samples of PBD-2-75 and PBD-3-75, both having a 0.75 weight fraction of hard segment but different HTPBD molecular weights. The OsO_4-stained soft-segment microdomains (dark domains) in both materials are dispersed in the hard-segment matrix which becomes the majority phase. The only significant difference between these two samples is that the size of the soft-segment microdomains in PBD-2-75 appears to be slightly smaller. One cannot distinguish whether the dispersed soft-segment microdomains are spherical, cylindrical, or platelike in character from a single EM image. To answer this question, HVEM images were recorded at various angles of tilt. Parts a and c of Figure 9 show HVEM micrographs at large tilt angles of $-20°$ and $+37°$, respectively, which are to be compared to the same area at zero tilt angle shown in Figure 9b. Parts a and c of Figure 9 show that the soft-segment microdomain dimension along the tilt direction appears shorter while the dimension perpendicular to tilt remains unchanged. This suggests that the microdomains are changing their projections on the image plane as the sample is tilted. Thus, the soft-segment microdomains are not spherical as the projection of a sphere does not change with tilt. Since the polybutadiene soft-segment volume fractions in both PBD-2-75 and PBD-3-75 are about 0.32, it is impossible for the soft segments to form continuous rods or columns. It is more likely that the polybutadiene soft segments form dispersed platelike microdomains. The

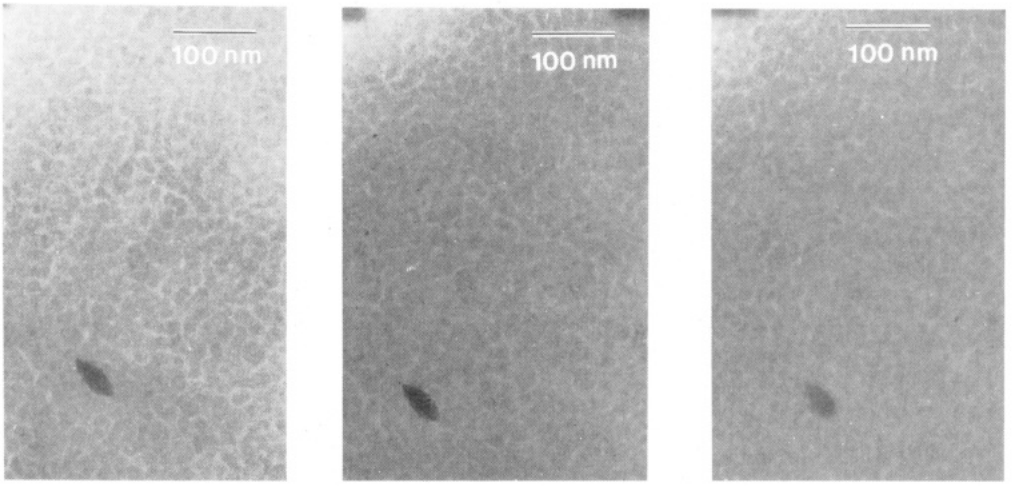

Figure 9. HVEM micrographs of PBD-2-75 at three specimen tilt angles: (a) −20°, (b) 0°, and (c) +37°.

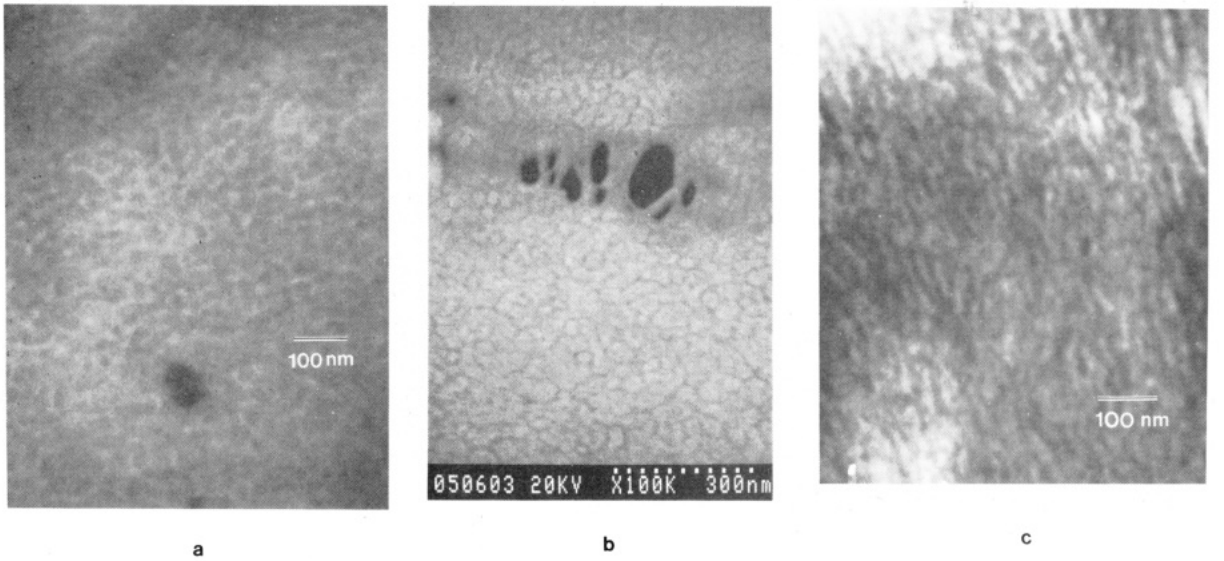

Figure 10. HVEM and SEM micrographs of OsO_4-stained PBD-3-75: (a) an HVEM micrograph of a solvent cast thin film, (b) a BSE SEM micrograph of the same thin film, (c) an HVEM micrograph of an ultramicrotomed thin section.

platelike microdomains will change their projections as the specimen is tilted.

High-resolution SEM backscattered electron and secondary electron images of thin films of PBD-3-75 are shown in Figure 10b and in Figure 11. These SEM images reconfirm the morphology observed from the HVEM but also show the potential of applying high-resolution SEM to characterize the block copolymer morphology. Note that contrast is reversed between the HVEM and SEM micrographs since, in SEM, the OsO_4-stained PBD soft-segment microdomains produce more secondary and backscattered electrons. Thus the stained areas appear brighter due to a stronger signal received by the various detectors in SEM. The microdomain sizes in the SEM micrograph agree with those in HVEM micrographs. In a recently completed low voltage high-resolution scanning electron microscopy study,[43] surface phase separation of soft- and hard-segment microdomains were observed in a thin film specimen of PBD-2-75 from a SEM micrograph. The air-polymer surface of PBD-2-75 contained PBD microdomains dispersed in a hard-segment matrix.[43] Plate or short columnlike PBD microdomains best described the morphology of the solvent cast thin films of PBD-2-75 and PBD-3-75.[43]

There are significant differences between morphologies observed from ultramicrotomed sections and from solvent

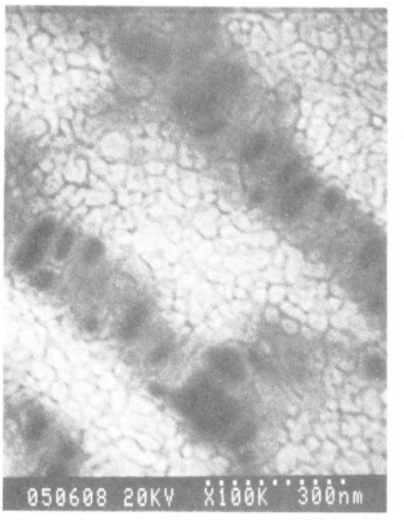

Figure 11. Secondary electron image SEM micrograph of a solvent cast PBD-3-75 film at 20 kV.

cast films of PBD-3-75 in comparison of Figure 10a–c. Figure 10c shows disordered short cylinders of soft-segment embedded in the MDI-BD hard-segment matrix that are characteristic of the bulk morphology represented by the ultramicrotomed section.[30] We also observed that PBD-

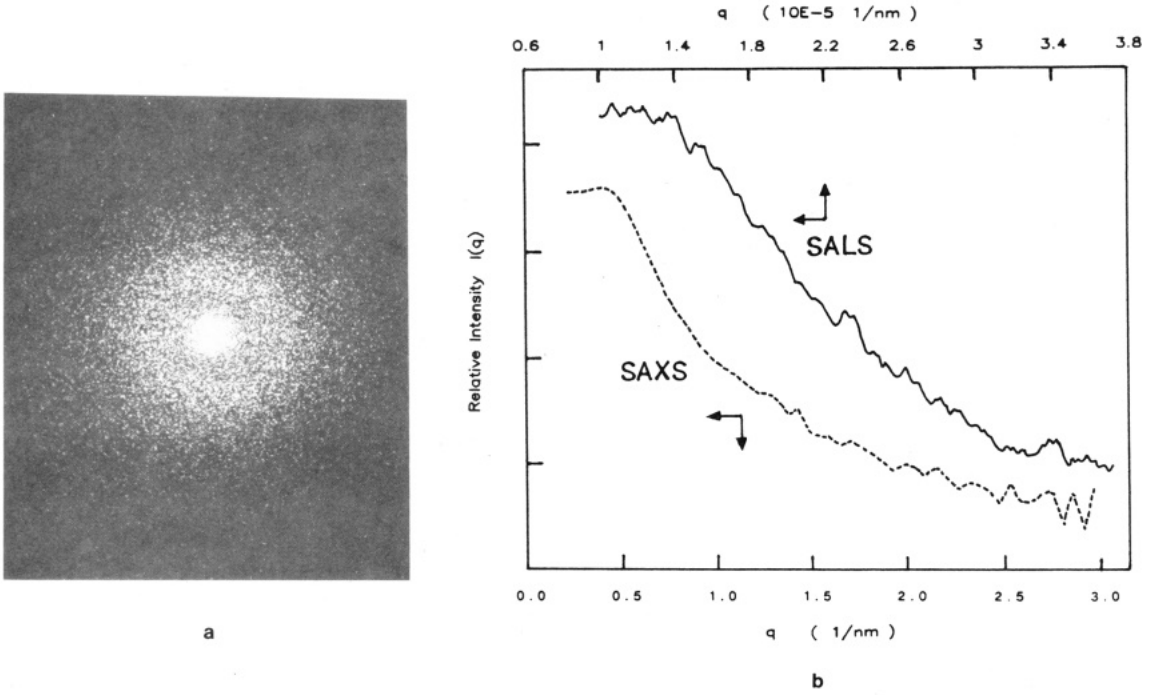

Figure 12. (a) Optical diffraction (SALS) pattern of an HVEM micrograph of PBD-3-75 and (b) SAXS and SALS curves of PBD-3-75 (the SALS curve was obtained by digitizing and radial averaging of the SALS pattern of PBD-3-75 shown in (a)).

2-75 exhibited a similar bulk morphology to that of PBD-3-75. These results are similar to the case of sample PBD-3-67 described earlier in that the cast film appear to have a more well-defined microphase separation.

The SAXS curve of PBD-3-75 in Figure 12b shows a single peak, typical of microphase-separated polyurethane scattering profiles. PBD-2-75 shows a similar SAXS pattern and is omitted from the figure. The long spacings of PBD-2-75 and PBD-3-75 are 22.3 and 27.1 nm, respectively (Table II). The long spacing cannot be interpreted directly as an interdomain distance since there is no evidence for a lamellar structure. To correlate SAXS profiles with the electron microscopy, we employed the method of optical diffractometry. Since the wavelength of a He–Ne laser is about 4000 times longer than that of a X-ray radiation, by using low magnification HVEM micrographs (photographically reduced), the relation between the dimensions of the scattering inhomogeneities and the wavelength of the radiation become comparable. Therefore, it is possible to obtain a light scattering pattern from an electron micrograph of the polyurethane morphology and compare it to the SAXS profile of the same material. An optical diffraction pattern of an HVEM micrograph of PBD-2-75 is shown in Figure 12a. Figure 12b shows a radially averaged relative intensity $I(q)$ versus scattering vector q curve obtained from the digitized optical diffraction pattern in Figure 12a. The light scattering profile also shows a single scattering peak similar to that of the SAXS curve plotted on the same graph. The long spacing calculated from the light scattering experiment of the HVEM micrograph corresponds very well to that calculated from SAXS profile after correcting for the wavelength differences in the scattering radiation and the HVEM magnification. This provides supporting evidence that the structure observed by HVEM is representative of the polymer morphology.

Summary

Segmented polybutadiene–polyurethane morphology was investigated by employing high-voltage transmission electron microscopy, high-resolution scanning electron microscopy with both secondary and backscattered electron imaging, and small-angle X-ray scattering. A rodlike or lamellar structure was observed in the PBD–polyurethanes when the hard-segment weight fraction varied from 0.42 to 0.67. The three-dimensional rodlike or lamellar morphology is bicontinuous with both phases interwoven and possessing high interconnectivity. It was also observed that thin film casting and ultramicrotomy techniques revealed similar morphology in this range of composition. At very low hard-segment content (0.31 wt fraction or lower), the hard-segment phase is dispersed in a matrix of soft segments. In this case the dispersed hard-segment microdomains could be either short cylinders or spheroids. At very high hard-segment contents, isolated polybutadiene soft-segment microdomains are embedded in a hard-segment matrix. The morphology observed in thin cast films of PBD-3-75 and PBD-2-75 differed significantly from that observed in thin sections of these two materials. Platelike PBD soft-segment microdomains are present in the thin films while randomly oriented soft-segment short cylinders were characteristic of the morphology of the microtomed samples. Optical diffraction patterns obtained from electron micrographs confirmed that the spacings of the microdomains observed with HVEM and SEM were comparable to those determined from X-ray scattering.

Acknowledgment. The authors acknowledge the stimulating discussions and excellent technical support of Drs. James B. Pawley, Peter H. Cooke, and Ester Szoke and Mr. Alan R. Kutchera of the NIH-Integrated Microscopy Resource at the University of Wisconsin—Madison. Howard W. Bielich deserves our thanks for writing the image analysis software. Hydroxyl-terminated polybutadiene oligomers were kindly provided by Dr. Suichi Matsumoto of Japan Synthetic Rubber Co., Japan. Professor Xuehai Yu of Nanjing University, PRC, synthesized two of the PBD–polyurethanes (PBD-2-75 and PBD-3-75) for this study. Funding of this work was provided by the National Science Foundation (DMR-8603839), the Office of Naval Research (N00014-83-

K0423), and the National Health Institute (HL-37351 and HL-21001). S.L.G. would like to thank the American Heart Association—Wisconsin Affiliate—for providing fellowship support.

References and Notes

(1) Cooper, S. L.; Tobolsky, A. V. *J. Appl. Polym. Sci.* **1966**, *10*, 1837.
(2) Allport, D. C., Janes, W. H., Eds. *Block Copolymers*; Wiley: New York, 1973.
(3) Estes, G. M.; Cooper, S. L. *Macromolecules* **1971**, *4*, 452.
(4) Seymour, R. W.; Cooper, S. L. *Rubber Chem. Technol.* **1974**, *47*, 19.
(5) Brunette, C. M.; Hsu, S. L.; Rossman, M.; MacKnight, W. J.; Scheider, N. S. *Polym. Eng. Sci.* **1981**, *21*, 668.
(6) Gibson, P. E.; Vallance, M. A.; Cooper, S. L. In *Developments in Block Copolymers-1*; Goodman, I., Ed.; Applied Science: London, 1982.
(7) Fridman, I. D.; Thomas, E. L. *Polymer* **1980**, *21*, 388.
(8) Bonart, R. *J. Macromol. Sci., Phys.* **1968**, *B2*, 1, 115.
(9) Clough, S. B.; Schneider, N. S.; King, A. O. *J. Macromol Sci., Phys.* **1968**, *B2*, 641.
(10) Samuels, S. L.; Wilkes, G. L. *J. Polym. Sci. Symp.* **1973**, *43*, 149.
(11) Schneider, N. S.; Desper, C. R.; Illinger, J. L.; King, A. O.; Barr, D. *J. Macromol Sci., Phys.* **1975**, *B11*, 5.
(12) Van Bogart, J. W. C. Ph.D. Thesis, University of Wisconsin, 1981.
(13) Speckhard, T. A.; Ver Strate, G.; Gibson, P. E.; Cooper, S. L. *Polym. Eng. Sci.* **1983**, *23*, 337.
(14) Chang, Y. J. P.; Wilkes, G. L. *J. Polym. Sci., Polym. Phys. Ed.* **1975**, *13*, 455.
(15) Hesketh, T. R.; Van Bogart, J. W. C.; Cooper, S. L. *Polym. Eng. Sci.* **1980**, *20*, 3, 190.
(16) Lagasse, R. R. *J. Appl. Polym. Sci.* **1977**, *21*, 2489.
(17) Chang, A. L.; Thomas, E. L. In *Multiphase Polymers*; Cooper, S. L., Estes, G. M., Eds.; American Chemical Society: Washington, DC, 1979. Briber, R. M.; Thomas, E. L. *J. Macromol. Sci., Phys.* **1983**, *B22*, 509.
(18) Wilkes, G. L.; Samuels, S. L.; Crystal, R. *J. Macromol. Sci., Phys.* **1974**, *B10*, 203.
(19) Koutsky, J. A.; Hein, N. V.; Cooper, S. L. *J. Polym. Sci., Polym. Lett. Ed.* **1970**, *8*, 353.
(20) Cowie, J. M. G. In *Developments in Block Copolymers*; Goodman, I., Ed.; Applied Science: London, 1982.
(21) Roche, E. J.; Thomas, E. L. *Polymer* **1981**, *22*, 333.
(22) Handlin, D. L.; MacKnight, W. J.; Thomas, E. L. *Macromolecules* **1980**, *14*, 795.
(23) Kato, K. *Polym. Eng. Sci.* **1967**, *7*, 38.
(24) Galeski, A.; Argon, A. S.; Cohen, R. E. *Makromol. Chem.*, submitted for publication.
(25) Pawley, J. B. *Ultramicroscopy* **1984**, *13*, 387.
(26) Berry, V. K. *Proc. EMSA* **1987**, 468.
(27) Foks, J.; Michler, G. *J. Appl. Polym. Sci.* **1986**, *31*, 1281.
(28) Pawley, J. B.; Scala, W. R. *Proc. EMSA* **1986**, 654.
(29) Chen, C. H. Y.; Briber, R. M.; Thomas, E. L.; Xu, M.; MacKnight, W. J. *Polymer* **1983**, *24*, 1333.
(30) Chen-Tsai, C. H. Y.; Thomas, E. L.; MacKnight, W. J.; Schneider, N. S. *Polymer* **1986**, *27*, 659.
(31) Serrano, M.; Ottino, J. M.; Thomas, E. L.; MacKnight, W. J. *Polymer* **1987**, *28*, 1667.
(32) Ogata, S.; Maeda, H.; Kakimoto, M.; Imai, Y. *J. Appl. Polym. Sci.* **1987**, *33*, 775.
(33) Goodman, S. L.; Li, C.; Albrecht, R. M.; Cooper, S. L. *Abstr. 61st Colloid Surf. Sci. Symp.* **1987**, 220.
(34) Cullity, B. D. *Elements of X-Ray Diffraction*, 2nd ed.; Addison-Wesley: Reading, 1978; pp 127–131.
(35) Li, C.; Cooper, S. L. *Bull. Am. Phys. Soc.* **1987**, *32*, 664.
(36) Dieterich, D. In *Polyurethane Handbook*; Oertel, G., Ed.; Hansen: New York, 1985; pp 19–22.
(37) Hepburn, C. *Polyurethane Elastomers*; Applied Science: New York, 1982; Chapter 2, pp 27–48.
(38) Goodman, S. L.; Albrecht, R. M. *Scanning Microsc.* **1987**, *1*, 727.
(39) Pawley, J. B. *Proc. EMSA* **1987**, 550.
(40) Kinning, D. J.; Thomas, E. L. *Macromolecules* **1984**, *17*, 1712.
(41) Hasegawa, T.; Hashimoto, T. *Macromolecules* **1985**, *18*, 589.
(42) Kinning, D. J.; Thomas, E. L.; Ottino, J. L. *Macromolecules* **1987**, *20*, 1129.
(43) Goodman, S. L.; Li, C.; Pawley, J. B.; Cooper, S. L.; Albrecht, R. M. In *Progress in Biomedical Engineering*; Ratner, B. D., Ed.; Elsevier: Amsterdam, 1988; in press.

Crystal Structure and Morphology of Syndiotactic Polypropylene Single Crystals

Bernard Lotz,*[1] Andrew J. Lovinger,* and Rudolf E. Cais

AT&T Bell Laboratories, Murray Hill, New Jersey 07974. *Received October 23, 1987*

ABSTRACT: Large, highly regular single crystals of syndiotactic polypropylene (sPP), grown for the first time and examined by electron microscopy and electron diffraction, reveal extra reflections and characteristic streaks that had not been reported in the published X-ray fiber structure analysis of Corradini, Natta, et al.[2] On the basis of these findings, we propose that the unit cell in these crystals is orthorhombic with a = 14.50 Å, b = 11.20 Å, c = 7.40 Å, space group *Ibca*; this unit cell has a strong subcell with b = 5.60 Å. The new cell symmetry results from the presence of *both* left- *and* right-handed helices, while the earlier unit cell[2] (having the $C222_1$ space group) is based upon helices that are *all* of the *same* hand. We show that in actual crystals both packing schemes coexist leading to intermolecular-lattice disorder and thereby to the observed streaking during electron diffraction. The habit of sPP single crystals is rectangular with the b axis of the unit cell parallel to the long dimension of the crystals.

Introduction

The crystal structure and morphology of syndiotactic polypropylene (sPP) have been investigated less than those of its isotactic counterpart (iPP). Corradini et al.[2] reported the crystal structure and molecular conformation of sPP in 1967. The molecular conformation is unusual in that the sequence of rotation angles *ggttggtt* implies that successive CH_2 groups have significantly different environments, a feature amply confirmed by NMR investigations.[3] The proposed unit cell[2] is orthorhombic with parameters a = 14.50 Å, b = 5.60 Å, c (fiber axis) = 7.40 Å, and space group $C222_1$; this space group preserves in the lattice all the symmetry elements of the polymer chains. Single crystals of sPP, grown from a variety of solvents by Marchetti and Martuscelli,[4] were elongated, but their lifetimes under the electron beam were reportedly too short to enable a diffraction investigation, so that the structure-morphology relationship could not be established unequivocally.

We report in this paper an electron microscopic and electron diffraction investigation of single crystals of sPP produced by thin-film growth. The diffraction patterns

0024-9297/88/2221-2375$01.50/0